Acta Pharmacologica Sinica (2015) 36: 847–854
 1671-4083/15
www.nature.com/aps

Original Article

Pharmacokinetics of PEGylated recombinant human endostatin (M_2ES) in rats

Zuo-gang LI[6, #], Lin JIA[3, 4, 5, #], Li-fang GUO[1, 2, #], Min YU[6], Xu SUN[6], Wen NIE[6], Yan FU[3, 4, 5], Chun-ming RAO[2], Jun-zhi WANG[2, *], Yong-zhang LUO[3, 4, 5, *]

[1]Peking Union Medical College; [2]National Institutes for Food and Drug Control; [3]National Engineering Laboratory for Anti-tumor Protein Therapeutics; [4]Beijing Key Laboratory for Protein Therapeutics; [5]Cancer Biology Laboratory, School of Life Sciences, Tsinghua University, Beijing 100084, China; [6]China's National Center for Safety Evaluation of Drugs, Beijing 100050, China

Aim: M_2ES is PEGylated recombinant human endostatin. In this study we investigated the pharmacokinetics, tissue distribution, and excretion of M_2ES in rats.
Methods: ^{125}I-radiolabeled M_2ES was administered to rats by intravenous bolus injection at 3 mg/kg. The pharmacokinetics, tissue distribution and excretion of M_2ES were investigated using the trichloroacetic acid (TCA) precipitation method.
Results: The serum M_2ES concentration-time curve after a single intravenous dose of 3 mg/kg in rats was fitted with a non-compartment model. The pharmacokinetic parameters were evaluated as follows: C_{max}=28.3 μg·equ/mL, $t_{1/2}$=71.5 h, $AUC_{(0-\infty)}$=174.6 μg·equ·h/mL, Cl=17.2 mL·h^{-1}·kg^{-1}, MRT=57.6 h, and V_{ss}=989.8 mL/kg for the total radioactivity; C_{max}=30.3 μg·equ/mL, $t_{1/2}$=60.1 h, $AUC_{(0-\infty)}$=146.2 μg·equ·h/mL, Cl=20.6 mL·h^{-1}·kg^{-1}, MRT=47.4 h, and V_{ss}=974.6 mL/kg for the TCA precipitate radioactivity. M_2ES was rapidly and widely distributed in various tissues and showed substantial deposition in kidney, adrenal gland, lung, spleen, bladder and liver. The radioactivity recovered in the urine and feces by 432 h post-dose was 71.3% and 8.3%, respectively. Only 0.98% of radioactivity was excreted in the bile by 24 h post-dose.
Conclusion: PEG modification substantially prolongs the circulation time of recombinant human endostatin and effectively improves its pharmacokinetic behavior. M_2ES is extensively distributed in most tissues of rats, including kidney, adrenal gland, lung, spleen, bladder and liver. Urinary excretion was the major elimination route for M_2ES.

Keywords: recombinant human endostatin; PEGylation; trichloroacetic acid precipitation method; pharmacokinetics; drug tissue distribution; drug excretion; rats

Acta Pharmacologica Sinica (2015) 36: 847–854; doi: 10.1038/aps.2015.16; published online 1 June 2015

Introduction

Endostatin, a 20-kDa proteolytic fragment of collagen XVIII, is a potent endogenous angiogenesis inhibitor isolated from supernatant of a murine hemangioendothelioma cell line[1]. It has been widely reported that endostatin has potent inhibitory effects on endothelial cell proliferation, migration, and tube formation[2, 3]. Nucleolin, integrins, caveolin and clathrin have been demonstrated to mediate the anti-tumor effects of endostatin[4–6]. Except in endothelial cells, endostatin also has anti-tumor lymphangiogenic and anti-lymphatic metastasis functions[7–9], further supporting the conclusion that endostatin is a potent anti-tumor drug with the potential ability to restrict tumor progression and metastasis[10].

Endostatin shows a broad anti-cancer spectrum and a low toxicity in animal models[11]. Systematic administration of rh-endostatin suppressed the growth of a number of primary tumors in mice, including Lewis lung carcinoma, T241 fibrosarcoma, B16F10 melanoma[12] and renal cell carcinoma[13], without the development of resistance or apparent toxicity. However, the clinical trials of rh-endostatin were terminated at the early phase II stage given production problems and unsatisfactory therapeutic effects[14]. In 2005, ZBP-Endostatin (zinc-binding peptide-Endostatin), a modified recombinant human endostatin, was approved by China Food and Drug Administration (CFDA) for the treatment of non-small-cell lung cancer (NSCLC)[15]. ZBP-Endostatin expressed by *Escherichia coli* has

# These authors contributed equally to this work.
* To whom correspondence should be addressed.
E-mail yluo@mail.tsinghua.edu.cn (Yong-zhang LUO);
wangjz@nicpbp.org.cn (Jun-zhi WANG)
Received 2014-11-04 Accepted 2015-02-27

been engineered to contain an additional nine-amino on its N terminus, which has been proved to enhance protein purification, solubility and stability. Because the rh-endostatin produced in the United States suffered from N-terminal truncations during Pichia pastoris expression, we speculate that both the N-terminus integrity and correct folding are critical for the stability and biological functions of endostatin[16, 17].

In clinical trials, endostatin monotherapy showed evident anti-tumor efficacy[18, 19] and exhibited a synergic activity with a favorable toxic profile in combination with chemotherapy[20]. However, the stability and retention of endostatin in the circulation were observed to be limited[21–23]. To reduce the administration frequency and to prolong its half-life, we modified recombinant human endostatin at the N-terminus by conjugation with a methoxy polyethylene glycol aldehyde called M_2ES[24]. PEGylation is one of the most extensively studied strategies, and it aims to improve the pharmacokinetic behavior of the therapeutic drugs by increasing the molecular mass of proteins and peptides, shielding them from proteolytic enzymes, prolonging *in vivo* circulating half-lives, lowering clearance and reducing their immunogenicity and antigenicity[25]. Currently, several therapeutic proteins, such as interferon-α2b[26], interleukin-6[27], and granulocyte colony-stimulating factor[28], have been PEGylated. Therefore, the chemical modification of recombinant human endostatin with PEG may potentially increase its drug efficacy.

In this study, the pharmacokinetics of M_2ES following intravenous injection were evaluated via an isotype-labeled assay. The tissue distribution and excretion pattern of M_2ES in rats were also investigated.

Materials and methods

Chemicals and reagents

M_2ES recombinant endostatin (rhES) solution (10–20 mg/mL, pH 5.2–5.3), supplemented with $NaBH_3CN$ (20 mmol/L) and PEG 2000 (PEG: rhES=1.5:1) at 37 °C for 4 h, was produced by fermentation [*Escherichia coli* BL21(DE3) strain] on a commercial scale (Protgen Ltd, Beijing, China)[24]. The purity and activity of M_2ES were more than 98% and 310 U/mL, respectively[24]. High specific activity, carrier-free protein iodination $Na^{125}I$ (purity>99.5%, 644 GBq/mg) was purchased from Amersham (Amersham, UK). The iodogen iodination reagent and bicinchoninic acid protein determination kit were obtained from Sigma (St Louis, MO, USA). The other reagents and solvents used in this study were of analytical grade.

Animals

Wistar rats (male and female, certificate D01-3031) were provided by the Experimental Animal Center of the Academy of Military Medical Sciences (Beijing, China). One rat was housed per cage. The rooms in which the animals were housed were controlled for temperature and humidity and maintained on a 12 h light/dark cycle. The animals had free access to a standard laboratory diet and water during the acclimation period before the experiments.

Preparation of ^{125}I-labeled PEGylated recombinant human endostatin

The M_2ES was radiolabeled according to the IodoGen method as previously described[29]. Briefly, 5.9 mg protein was incubated with 5 mCi $Na^{125}I$ in a calibrated reaction vial coated with 100 μg of iodogen reagent with gentle stirring for 12 min at 20 °C. After incubation, the iodinated protein was purified on a Sephacryl S200H gel column at a flow rate of 1 mL/h with 20 mmol/L Tris buffer (pH 7.4) to separate the free ^{125}I from the protein-bound ^{125}I. Column fractions were collected at 3-min intervals. The radioactivity of each eluted fraction was determined by the assembled γ counter. The concentrations of ^{125}I-labeled M_2ES were determined by using the bicinchoninic acid assay according to the instructions of the manufacturer. The fractions containing ^{125}I-labeled M_2ES were combined. The radiochemical purity of the ^{125}I-labeled M_2ES was determined by size-exclusive high performance liquid chromatography (SHPLC) with Superdex™ peptide 10/300GL and 0.1 mol/L NaAc buffer (pH4.0) at a flow rate of 0.5 mL/min. The radio-chromatogram was obtained from a HP1100 system with a detector of Packard Radiomatic™ Flow Scintillation Analyzer 525TR (Meriden, CT, USA).

Determination of ^{125}I-labeled M_2ES activity

Cell migration was assessed using a modified Boyden chamber (8 μm pores, Costar). HUVEC (2.4×10^5 cells in 100 μL) were seeded in the upper chambers. M_2ES and ^{125}I-labeled M_2ES from 33rd and 31st eluted fractions at indicated concentrations were added in the lower chamber. Dulbecco's modified Eagle's medium (DMEM) supplemented with 1% serum was used as the control. After incubation for 6 h at 37 °C, the migrated cells were quantified by counting in randomly selected fields of each chamber. Each experiment was analyzed in triplicate.

Validation of the radioactivity determination by a TCA precipitation assay

The calibration curves were generated by adding a series of concentrations of ^{125}I-labeled M_2ES (0.0257–16.08 ng/μL) into the blank plasma, tissues and excreta samples. After 20% TCA precipitation, the radioactivities of the samples were measured. The results (data not shown) showed good linearity (r^2>0.999) and precision (CV%<10%) for all samples. The ratios of radioactivity recovered from the TCA precipitated pellet were more than 90% of the added radioactivity, indicating that the ^{125}I-labeled M_2ES mainly existed in the TCA precipitants. Therefore, the TCA precipitation method was confirmed to be accurate, reliable and reproducible.

Pharmacokinetic study

Six Wistar rats (thee males and thee females, 250±10 g) were injected with ^{125}I-labeled M_2ES at a single dose of 3 mg/kg (4 MBq/kg) by iv injection via the tail vein. Blood samples were collected from the tail vein into heparinized tubes prior to administration and at 2, 4, 8, 12, 24, 72, 96, 120, 168, 216,

and 264 h after drug administration. Plasma samples in the volume of 50 μL were added with 400 μL 20% TCA to precipitate the proteins. After centrifugation, the radioactivities of precipitants and supernatants were detected to obtain the total radioactivity. The concentrations of ^{125}I-labeled M_2ES were expressed as microgram-equivalents per milliliter (μg·equ·mL^{-1}) compared to the injected drug specific activity.

Tissue distribution study

Twenty-four Wistar rats (twelve males and twelve females, 250±10 g) were randomly divided into 4 groups (n=6 per group) receiving a single iv bolus injection of ^{125}I-labeled M_2ES at 3 mg/kg (4 MBq/kg) via the tail vein. Blood and urine were collected and tissues were excised at 4, 36, 72, and 120 h post-dosing. The tissues included the thyroid, thymus, heart, lungs, liver, spleen, adrenal gland, kidney, bladder, testicle/uterus, intestinal contents, jejunum, adipose, muscle, bone marrow/thighbone and brain. All tissues or organs were individually weighed on an analytical balance and homogenized and then precipitated by adding 400 μL 20% TCA. After centrifugation, the radioactivities of precipitants and supernatants were detected and expressed as cpm/g or cpm/mL and Bq/g or Bq/mL, respectively. Then, the radioactivities of various tissues were expressed in weight, as microgram-equivalents per gram (μg·equ·g^{-1}), or in volume, as microgram-equivalents per milliliter (μg·equ·mL^{-1}), compared to the specific activity of injected drug. The total $AUC_{(0-120\ h)}$ and TCA precipitation $AUC_{(0-120\ h)}$ in various tissues were calculated in Windows Excel 7.0. The radioactivity distribution and AUC values in different tissues at indicated time points were analyzed.

Urinary and fecal excretion

Each of the rats (n=6, three males and three females, 250±10 g) received a single iv injection of ^{125}I-labeled M_2ES at 3 mg/kg (4 MBq/kg) and was then individually placed in a metabolic cage. The rats were provided standard food and water throughout the experiment. Total voided urine and excreted feces samples were collected from each rat at intervals of 0–24, 24–48, 48–72, 72–96, 96–120, 120–144, 144–168, 168–192, 192–216, 216–240, 240–264, 264–288, 288–336, 336–360, 360–384, 384–408, and 408–432 h post-dosing. The samples were analyzed for γ-radioactivity, such that the percentage of accumulated radioactivity to total radioactivity could be calculated.

Biliary excretion

Briefly, the experimental rats (n=5, two males and three females, 250±10 g) were anesthetized by ip injection with 10% chloral hydrate supplemented with ether. Following a midline abdominal incision, the common bile duct was exposed and the distal end ligated with a silk suture. The bile duct was cannulated with PE tubing for the collection of bile samples. ^{125}I-labeled M_2ES was administered as a single iv injection at 3 mg/kg (4 MBq/kg). The bile was collected at an intervals of 1 h over 12 h, and the volume of each collected sample was recorded separately. Thereafter, bile was collected over 12-h intervals (thus, the total collection period was 24 h). The ^{125}I radioactivities in the collected bile samples were determined by γ-radioactivity.

Statistical analysis

All data are expressed as the mean±standard deviation (SD). The pharmacokinetic analysis of the data was carried out using the non-compartmental model (Model: NCA 201) methods in WINNONLIN Version 2.1 to calculate the PK parameters. Differences in the numeric variables between the groups were assessed with a two-tailed t-test, and differences within the groups were assessed with a self-paired t-test. The data were fitted by linear regression, and the concentration-time curves were drawn with Microcal Origin software.

Results

Biological activity determination of ^{125}I-labeled M_2ES

The motility (the ratio of migrated cells in drug treatment group to control group) of the M_2ES group was 64.85%, while the ^{125}I-M_2ES with 10.39 kBq/μL radioactivity group showed 63.5% migratory inhibition and the ^{125}I-M_2ES with 11.37 kBq/μL radioactivity group showed 48.35% migratory inhibition, with P-values more than 0.05 compared to the motility of the M_2ES group. Therefore, ^{125}I-M_2ES was found to have a similar biological activity as unlabeled M_2ES, and no significant difference was observed, indicating that ^{125}I-labeling did not influence the activity of M_2ES.

Plasma pharmacokinetics of M_2ES in rats

The total plasma radioactivity and TCA precipitant radioactivity versus time after single iv injection at dose of 3 mg/kg are depicted in Figure 1A. The results show that no significant differences (P>0.05) were observed between the total plasma radioactivity concentration and the TCA precipitant radioactivity concentration before 168 h after drug injection. However, the total plasma radioactivity was significantly higher than the TCA precipitant radioactivity at 216 and 264 h following drug injection, indicating that small molecules of radiolabeled degradation products from parent drugs existed in the supernatants after 216 h. More than 80% of the total radioactivity was recovered in the TCA-precipitated pellets in the 2–120 h following drug injection. The ratio of the TCA precipitant radioactivity concentration to the total radioactivity concentration reached 60% at 264 h, suggesting that ^{125}I-labeled M_2ES degraded very slowly after iv administration. The corresponding pharmacokinetic parameters were generated by fitting plasma radioactivity concentration profiles to a non-compartmental model as shown in Table 1. The C_{max} of the total plasma radioactivity and TCA precipitant radioactivity after iv administration were 28.3±2.4 and 30.3±2.9 μg·equ·mL^{-1}, respectively. The $AUC_{(0-264\ h)}$ values of the total plasma radioactivity and TCA precipitant radioactivity were 166.6±7.6 and 142.0±6.5 μg·equ·h·mL^{-1}. The clearance (Cl) values were 17.2±0.9 and 20.6±1.0 mL·h^{-1}·kg^{-1}, the terminal elimination half-life ($t_{1/2}$) values were 71.5±7.6 and 60.1±7.8 h, the mean residence time (MRT) values were 57.6±5.0 and 47.4±5.2 h, and the V_{SS} values were 989.8±81.6 and 974.6±109.5

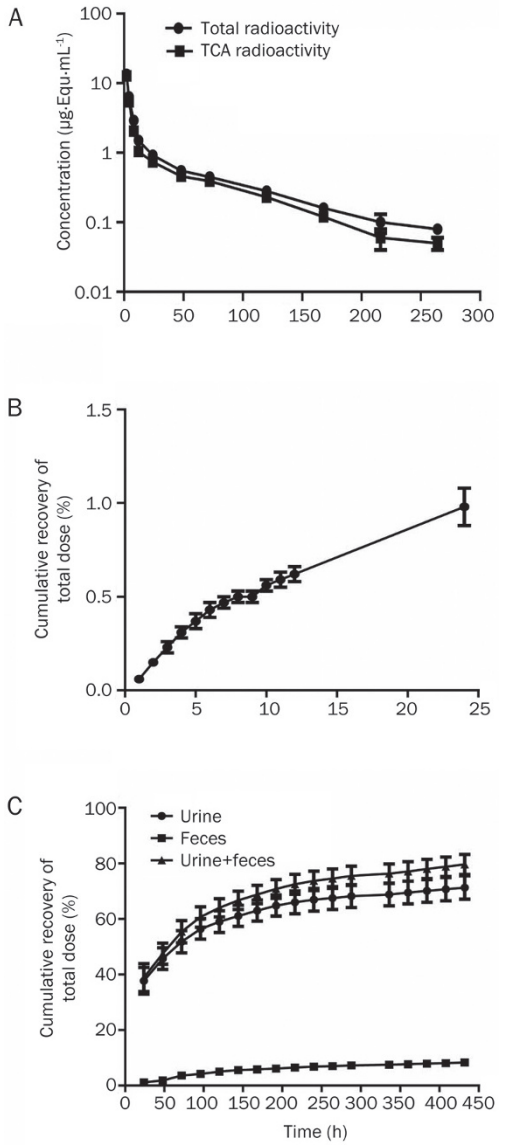

Figure 1. Concentration-time curves and cumulative total radioactivity of M_2ES. (A) Concentration-time curves of M_2ES after a single iv injection at a dose of 3 mg/kg in rats. The data are expressed as the mean±SD. *n*=6. (B) Cumulative total radioactivity recovered from bile following a single iv injection of 3 mg/kg M_2ES. The data are expressed as the mean±SD. *n*=6. (C) Cumulative total radioactivity recovered from urine and feces following a single iv injection of 3 mg/kg M_2ES. The data are expressed as the mean±SD. *n*=6.

mL/kg for the total plasma radioactivity and TCA precipitant radioactivity, respectively.

Mass balance study and the biliary excretion of M_2ES

After the iv administration of ^{125}I-M_2ES to the bile-duct cannulated rats, only 0.98% of the dosed radioactivity was excreted into bile by 24 h post-dosing (Figure 1B), indicating that biliary excretion is a minor pathway for ^{125}I-M_2ES in rats.

The urinary and fecal excretions of ^{125}I-M_2ES in rats were also investigated following a single iv administration at a dosage of 3 mg/kg (4 MBq/kg) to the bile duct intact rats. The results showed that urinary excretion was the dominant route of elimination following iv administration (Figure 1C) because the accumulative urinary excretion of ^{125}I-M_2ES reached 59% of the administered radioactivity after 120 h post-dosing, while the cumulative fecal excretion was only 5.0%. Over the 432 h collection period, a mean of 79.6% of the radioactive dose was recovered from the excreta. The bulk (71.3%) was eliminated in the urine, and only a minority (8.3%) was eliminated in the feces.

Table 1. Pharmacokinetic parameters of ^{125}I-M_2ES after single iv administration at the dose of 3 mg/kg in rats. Data are expressed as mean±SD. *n*=6.

Parameter	Unit	Total radioactivity	TCA precipitant radioactivity	*P* value
C_{max}	μg·equ·mL^{-1}	28.3±2.4	30.3±2.9	0.2301
$t_{1/2}$	h	71.5±7.6	60.1±7.8	0.0277
$AUC_{(0-264\ h)}$	μg·equ·h·mL^{-1}	166.6±7.6	142.0±6.5	0.0001
$AUC_{(0-\infty)}$	μg·equ·h·mL^{-1}	174.6±8.7	146.2±6.9	0.0001
Cl	mL·h^{-1}·kg^{-1}	17.2±0.9	20.6±1.0	0.0001
MRT	h	57.6±5.0	47.4±5.2	0.0063
V_{ss}	mL/kg	989.8±81.6	974.6±109.5	0.7907

C_{max}, maximum plasma concentration; $t_{1/2}$, terminal elimination half-life; AUC, area under the plasma concentration versus time curve; Cl, systemic clearance; MRT, mean residence time; V_{ss}, volume of distribution at steady state. *P* values are obtained by evaluating the pharmacokinetic parameters between total plasma radioactivity and TCA precipitant radioactivity.

Tissue distribution of M_2ES in rats

After a single iv injection at a dose of 3 mg/kg in rats, the tissue distributions of ^{125}I-M_2ES at 4, 36, 72, and 120 h and the total radioactivity [$AUC_{(0-120\ h)}$] in the issues were evaluated (Figure 2). The radioactivity levels in order of AUC values from high to low were urine, kidney, adrenal gland, serum, lung, spleen, bladder, jejunum, intestinal contents, heart, liver, testicle/uterus, bone marrow/thighbone, thymus, muscle, adipose and brain. The radioactive ^{125}I-M_2ES showed substantial disposition in the urinary excretion system, highly perfused tissues and serum, while the radioactivity levels in the muscle, adipose and brain were the lowest. The radioactivity in the thyroid gland was only 0.0025%±0.0007% at 4 h and 0.0005%±0.0002% at 120 h of the dosed radioactivity after administration, which did not influence the reliability of the conclusions in the ^{125}I-M_2ES tissue distribution.

The radioactivity distribution at 4, 36, 72, and 120 h and the cumulative radioactivity in the TCA precipitant [$AUC_{(0-120\ h)}$] of tissues after a single iv injection of ^{125}I-M_2ES at a dose of 3 mg/kg are shown in Figure 3. The radioactivity levels of the issues from high to low according to the AUC values were kidney, adrenal gland, urine, serum, lung, spleen, bladder, liver, heart, jejunum, intestinal contents, testicle/uterus, bone

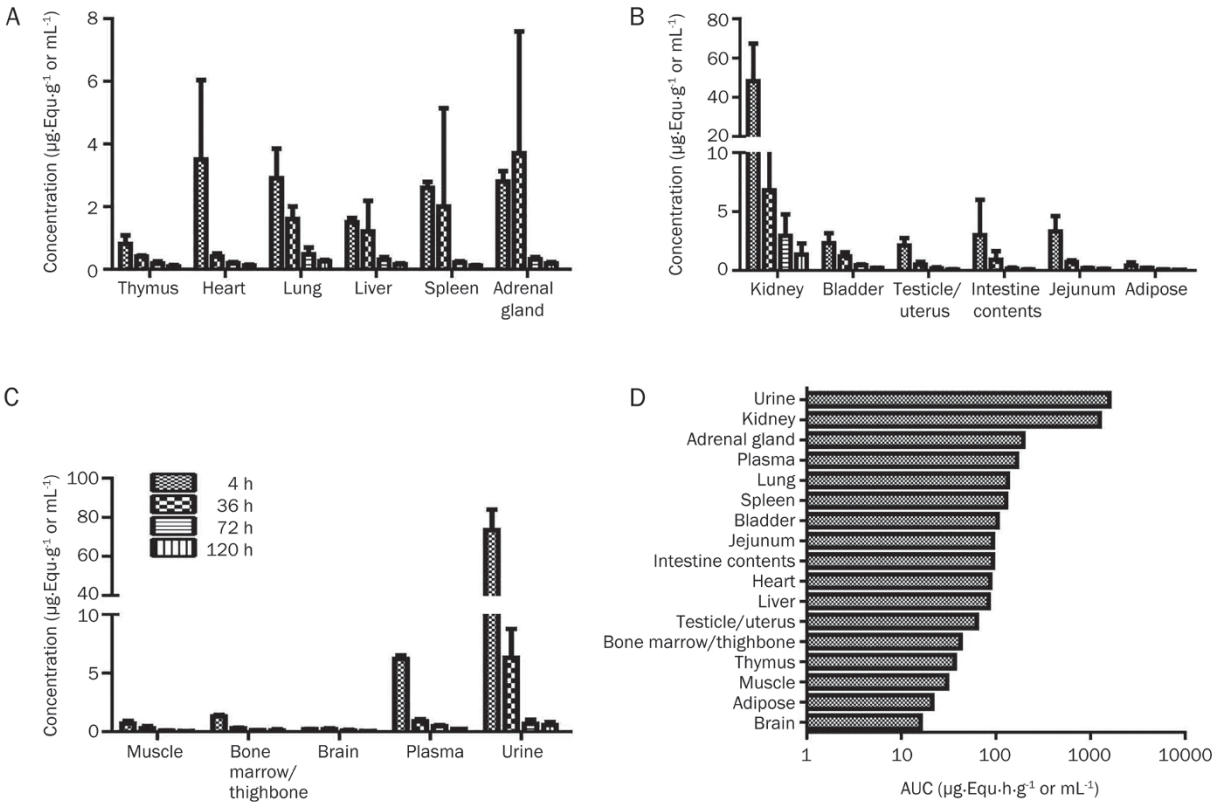

Figure 2. Tissue distributions of M_2ES. (A–C) The tissue distribution of total radioactivity at 4, 36, 72, and 120 h after a single iv administration of ^{125}I-M_2ES at a dose of 3 mg/kg in rats. The data are expressed as the mean±SD. *n*=6. (D) Distribution of total radioactivity [$AUC_{(0-120\ h)}$] in tissues after the iv administration of ^{125}I-M_2ES at a dose of 3 mg/kg in rats. *n*=6.

marrow/thighbone, muscle, thymus, adipose tissue and brain. With the exception of the kidney and adrenal gland samples, the highest deposition was found in the serum, which was consistent with the prediction that highly perfused tissues showed greater radioactivity. The radioactivities in adipose and brain were the lowest, and drugs were hardly transported across the blood-brain barrier. The radioactivities in most tissues reached the maximum level by 4 h after administration, decreased rapidly in the 4–36 h after dosing, and decreased slowly in the 72–120 h after dosing.

The ratio of the TCA precipitant radioactivity to the total radioactivity reflected the amounts of ^{125}I-M_2ES parent drug binding to various tissues. The ratios of TCA precipitant radioactivity to total radioactivity at different time points after drug injection are shown in Table 2. The data showed that 70%–90% of the additional radioactivity was recovered in the TCA precipitants in most tissues at 24 h after drug administration and 60%–90% at 120 h after dosing. The ratio of the TCA precipitant radioactivity to the total radioactivity in the serum remained greater than 74% over time, while the ratio of the TCA precipitant radioactivity to the total radioactivity in urine was approximately 7%–11%, indicating that urine mainly contained the soluble degradation products of ^{125}I-M_2ES.

Table 2. The ratio of TCA precipitant radioactivity to total radioactivity at 24, 48, 96, and 120 h after single iv administration of ^{125}I-M_2ES at the dose of 3 mg/kg in rats. *n*=5. Data are expressed as mean±SD.

Tissue	24 h (%)	48 h (%)	96 h (%)	120 h (%)
Thymus	63.8±6.9	55.0±4.7	67.1±9.3	62.3±10.4
Heart	87.6±3.9	69.3±2.7	79.5±5.4	74.6±4.3
Lung	82.7±10.3	83.0±5.9	71.5±23.2	74.4±4.4
Liver	75.1±6.7	80.1±10.1	88.3±3.1	85.8±3.9
Spleen	86.3±3.2	84.5±7.8	84.6±3.1	74.6±3.5
Adrenal gland	84.8±3.2	86.9±10.6	77.6±2.3	71.6±2.0
Kidney	92.2±1.1	94.2±2.4	95.2±2.0	92.2±3.9
Bladder	59.4±3.9	77.5±8.0	83.3±2.8	75.4±3.2
Testicle/uterus	79.5±8.3	62.8±12.2	79.6±3.9	72.8±6.1
Intestinal contents	36.7±12.9	59.2±18.8	67.3±8.5	60.9±6.2
Jejunum	66.7±11.7	71.2±9.4	74.7±6.6	65.7±7.1
Adipose	73.6±4.4	79.7±6.3	74.1±3.2	70.2±5.8
Muscle	70.2±12.1	74.6±2.4	74.4±4.4	71.8±3.1
Bone marrow/ thighbone	76.0±6.5	64.4±6.3	70.6±6.4	69.3±5.0
Brain	60.7±4.5	58.3±12.0	70.8±5.7	65.8±5.0
Plasma	86.7±4.0	74.0±4.4	87.7±3.2	85.1±3.8
Urine	9.7±7.8	10.3±4.1	7.4±3.3	10.7±2.7

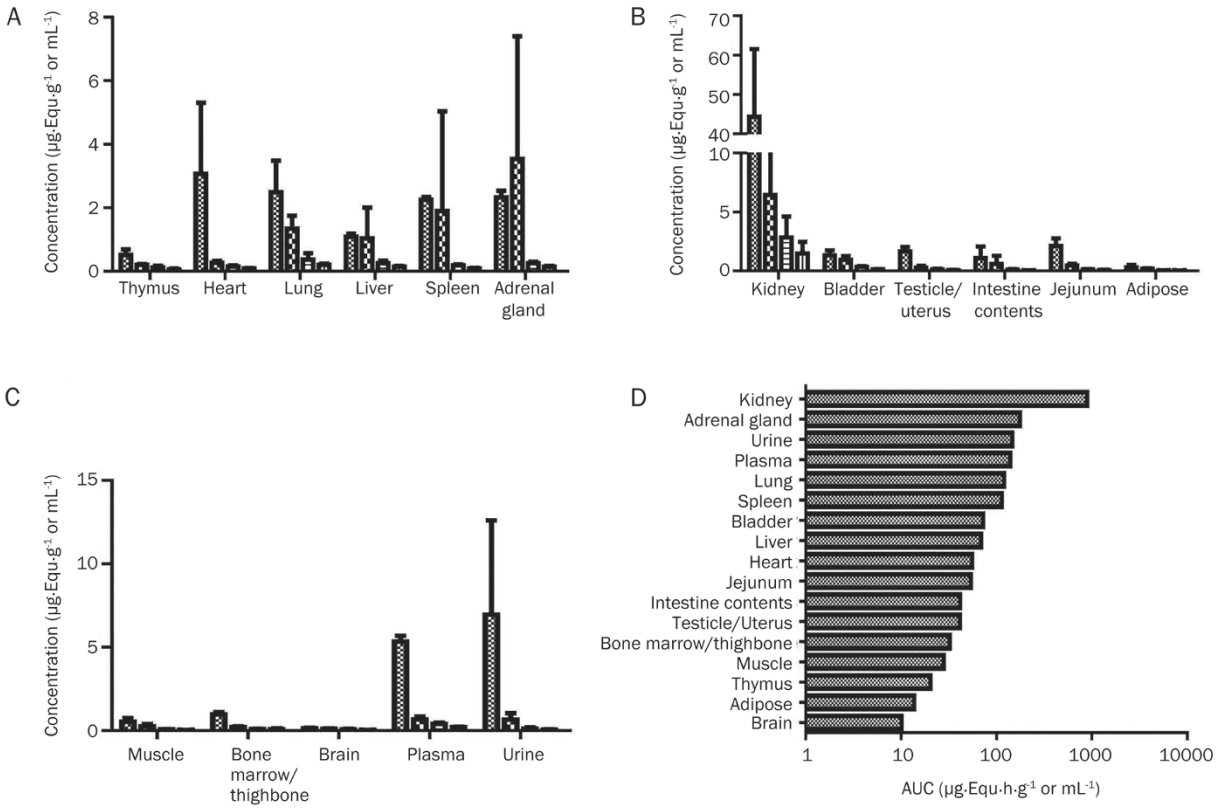

Figure 3. M_2ES tissue distribution. (A–C) The tissue distribution of TCA precipitant radioactivity at 4, 36, 72, and 120 h after single iv administration of ^{125}I-M_2ES at the dose of 3 mg/kg in rats. The data are expressed as the mean±SD. *n*=6. (D) Distribution of TCA precipitant radioactivity [$AUC_{(0-120\ h)}$] in tissues after the iv administration of ^{125}I-M_2ES at the dose of 3 mg/kg in rats. *n*=6.

Discussion

The evaluation of the pharmacokinetics profile, tissue distribution and excretion patterns for a novel drug are essential for its preclinical and clinical application. To the best of our knowledge, this is the first study to report the plasma pharmacokinetics, tissue distribution and excretion patterns for PEGylated rh-endostatin (M_2ES) in rats.

The TCA precipitation assay is a common method in the pharmacokinetic studies of protein drugs. In this study, the TCA precipitation radioactivity and the total radioactivity were measured to evaluate the M_2ES concentration in the plasma and in different tissues. Because the interference of free ^{125}I and soluble degradation products of ^{125}I-M_2ES was excluded, the results of TCA precipitation can better reflect the concentration of parent M_2ES. The radioactivity concentrations of ^{125}I-M_2ES in the TCA precipitants were lower than those in the total radioactivity concentrations in both the plasma and other tissues, but they followed approximately the same trend.

It has been reported that PEG conjugation can protect protein drugs against enzymatic digestion, slow their filtration by the kidneys and reduce the generation of neutralizing antibodies, therefore increasing the retention of the drugs in circulation. In previous studies, the pharmacokinetics of rh-endostatin were reported in rats and rhesus monkeys[30, 31]. The half-lives of rh-endostatins (4.5 mg/kg) in rats and in rhesus monkeys were 3.91 and 3.1 h, respectively. PEGylation significantly prolonged the half-life of rh-endostatin to 60.1 h at a dose of 3 mg/kg. Significant differences were also observed in Cl and $AUC_{(0-\infty)}$ among pharmacokinetics parameters between M_2ES in rats and rh-endostatin in rats and rhesus monkeys. The clearance of rh-endostatin (1.5 mg/kg) was 140.4 $mL\cdot h^{-1}\cdot kg^{-1}$ in rats and 110 $mL\cdot h^{-1}\cdot kg^{-1}$ in rhesus monkeys, while the clearance of M_2ES (3 mg/kg) in rats was 20.6 $mL\cdot h^{-1}\cdot kg^{-1}$, which was much slower than those of rh-endostatin in rats and rhesus monkeys. The slower disappearance of M_2ES resulted in greater values for the area under the serum concentration-time curve, with an $AUC_{(0-\infty)}$ value of 146.2±6.9 $\mu g\cdot equ\cdot h\cdot mL^{-1}$ at the dose of 3 mg/kg, compared to those of rh-endostatin (4.5 mg/kg) in rats and rhesus monkeys, which were 28.91 and 33 μg·h/mL, respectively. The comparison of the pharmacokinetic parameters of rh-endostatin and M_2ES demonstrated that PEGylation indeed improved rh-endostatin properties and prolonged its residence time in bodies. It may thereby improve its therapeutic potential.

The tissue distribution of M_2ES was investigated following a single iv administration in rats. Widely distributed radioactivities were observed in various tissues and organs within the time course examined. The levels of radioactivity in most tissues decreased rapidly over time. The $AUC_{(0-120\ h)}$ distribution

of individual tissues in the TCA precipitant peptide showed that except for plasma and urine, the majority of the radioactivity was detected in highly perfused tissues and organs, with the highest deposition levels detected in the kidney, followed by the adrenal gland, lung, spleen, bladder and liver. For the clearance organs, the kidney and liver showed high absorption levels of M_2ES, which were also reported in studies of rh-endostatin and other proteins such as angiostatin[32] and porcine fibrinogen[33]. In this study, the radioactivity detected in the kidneys was greater than that in the liver, indicating that the kidney played a more important role in the elimination of M_2ES and its metabolites, which was consistent with the results in the excretion studies showing that most M_2ES was eliminated in the urine. Therefore, monitoring renal function is necessary when M_2ES is used in the clinic, and adjusting the dosage is needed to avoid adverse effects in patients whose kidney functions are impaired. Moreover, high levels of radioactivity were also found in the lungs, and these decreased slowly compared to other tissues, which was similar to previous findings for rh-endostatin. This potentially provided evidence for the application of endostatin in the treatment of lung cancer.

In conclusion, we developed and validated a sensitive ^{125}I-labled method to investigate the pharmacokinetics, tissue distribution and excretion of M_2ES. According to our pharmacokinetic parameters, PEG conjugation significantly enhanced the circulation retention of rh-endostatin, resulting in a longer half-life ($t_{1/2}$) and slower clearance (Cl). Following intravenous injection, M_2ES was widely distributed in most tissues, and urinary excretion was the dominant route for elimination. The present pharmacokinetics study provides helpful information for the application of M_2ES in the clinical setting.

Acknowledgements

This work was supported by the National Science and Technology Major Project 2009ZX09306-002; Major Scientific and Technological Special Project for "Significant New Drug Creation" 2009ZX09102-243; and Protgen Ltd (Beijing, China).

Author contribution

Zuo-gang LI, Lin JIA, Li-fang GUO, Jun-zhi WANG, and Yong-zhang LUO designed the research; Zuo-gang LI, Lin JIA, Li-fang GUO, Min YU, Xu SUN, and Wen NIE performed the research; Zuo-gang LI, Lin JIA, Li-fang GUO, Yan FU and Chun-ming RAO analyzed the data; Zuo-gang LI, Lin JIA, Li-fang GUO, Jun-zhi WANG, and Yong-zhang LUO wrote the paper.

References

1 O'Reilly MS, Boehm T, Shing Y, Fukai N, Vasios G, Lane WS, *et al*. Endostatin: an endogenous inhibitor of angiogenesis and tumor growth. Cell 1997; 88: 277–85.

2 Taddei L, Chiarugi P, Brogelli L, Cirri P, Magnelli L, Raugei G, *et al*. Inhibitory effect of full-length human endostatin on *in vitro* angiogenesis. Biochem Biophys Res Commun 1999; 263: 340–5.

3 Shi H, Huang Y, Zhou H, Song X, Yuan S, Fu Y, *et al*. Nucleolin is a receptor that mediates antiangiogenic and antitumor activity of endostatin. Blood 2007; 110: 2899–906.

4 Chen Y, Wang S, Lu X, Zhang H, Fu Y, Luo Y. Cholesterol sequestration by nystatin enhances the uptake and activity of endostatin in endothelium via regulating distinct endocytic pathways. Blood 2011; 117: 6392–403.

5 Song N, Ding Y, Zhuo W, He T, Fu Z, Chen Y, *et al*. The nuclear translocation of endostatin is mediated by its receptor nucleolin in endothelial cells. Angiogenesis 2012; 15: 697–711.

6 Guo L, Song N, He T, Qi F, Zheng S, Xu XG, *et al*. Endostatin inhibits the tumorigenesis of hemangioendothelioma via downregulation of CXCL1. Mol Carcinog 2014. doi: 10.1002/mc.22210.

7 Ou J, Li J, Pan F, Xie G, Zhou Q, Huang H, *et al*. Endostatin suppresses colorectal tumor-induced lymphangiogenesis by inhibiting expression of fibronectin extra domain A and integrin alpha9. J Cell Biochem 2011; 112: 2106–14.

8 Brideau G, Makinen MJ, Elamaa H, Tu H, Nilsson G, Alitalo K, *et al*. Endostatin overexpression inhibits lymphangiogenesis and lymph node metastasis in mice. Cancer Res 2007; 67: 11528–35.

9 Zhuo W, Luo C, Wang X, Song X, Fu Y, Luo Y. Endostatin inhibits tumour lymphangiogenesis and lymphatic metastasis via cell surface nucleolin on lymphangiogenic endothelial cells. J Pathol 2010; 222: 249–60.

10 Zhuo W, Chen Y, Song X, Luo Y. Endostatin specifically targets both tumor blood vessels and lymphatic vessels. Front Med 2011; 5: 336–40.

11 Folkman J. Antiangiogenesis in cancer therapy — endostatin and its mechanisms of action. Exp Cell Res 2006; 312: 594–607.

12 Boehm T, Folkman J, Browder T, O'Reilly MS. Antiangiogenic therapy of experimental cancer does not induce acquired drug resistance. Nature 1997; 390: 404–7.

13 Dhanabal M, Ramchandran R, Volk R, Stillman IE, Lombardo M, Iruela-Arispe ML, *et al*. Endostatin: yeast production, mutants, and antitumor effect in renal cell carcinoma. Cancer Res 1999; 59: 189–97.

14 Whitworth A. Endostatin: are we waiting for Godot? J Natl Cancer Inst 2006; 98: 731–3.

15 Rong B, Yang S, Li W, Zhang W, Ming Z. Systematic review and meta-analysis of Endostar (rh-endostatin) combined with chemotherapy versus chemotherapy alone for treating advanced non-small cell lung cancer. World J Surg Oncol 2012; 10: 170.

16 Fu Y, Luo Y. The N-terminal integrity is critical for the stability and biological functions of endostatin. Biochemistry 2010; 49: 6420–9.

17 Fu Y, Tang H, Huang Y, Song N, Luo Y. Unraveling the mysteries of endostatin. IUBMB Life 2009; 61: 613–26.

18 Yang L, Wang JW, Tang ZM, Liu XW, Huang J, Li ST, *et al*. A phase I clinical trial for recombinant human endostatin. Chin J New Drugs 2004; 13: 548–53.

19 Yang L, Wang JW, Sun Y, Zhu YZ, Liu XQ, Li WL, *et al*. Randomized phase II trial on escalated doses of Rh-endostatin (YH-16) for advanced non-small cell lung cancer. Zhonghua Zhong Liu Za zhi 2006; 28: 138–41.

20 Wang J, Sun Y, Liu Y, Yu Q, Zhang Y, Li K, *et al*. Results of randomized, multicenter, double-blind phase III trial of rh-endostatin (YH-16) in treatment of advanced non-small cell lung cancer patients. Chin J Lung Cancer 2005; 8: 283–90.

21 Li Y, Huang XE, Yan PW, Jiang Y, Xiang J. Efficacy and safety of endostar combined with chemotherapy in patients with advanced solid tumors. Asian Pac J Cancer Prev 2010; 11: 1119–23.

22 Han B, Xiu Q, Wang H, Shen J, Gu A, Luo Y, *et al*. A multicenter, randomized, double-blind, placebo-controlled study to evaluate the efficacy of paclitaxel-carboplatin alone or with endostar for advanced

non-small cell lung cancer. J Thorac Oncol 2011; 6: 1104–9.
23 Cui C, Mao L, Chi Z, Si L, Sheng X, Kong Y, *et al*. A phase II, randomized, double-blind, placebo-controlled multicenter trial of Endostar in patients with metastatic melanoma. Mol Ther 2013; 21: 1456–63.
24 Guo L, Geng X, Chen Y, Qi F, Liu L, Miao Y, *et al*. Pre-clinical toxicokinetics and safety study of M_2ES, a PEGylated recombinant human endostatin, in rhesus monkeys. Regul Toxicol Pharmacol 2014; 69: 512–23.
25 Harris JM, Chess RB. Effect of pegylation on pharmaceuticals. Nat Rev Drug Discov 2003; 2: 214–21.
26 Glue P, Fang JW, Rouzier-Panis R, Raffanel C, Sabo R, Gupta SK, *et al*. Pegylated interferon-alpha2b: pharmacokinetics, pharmacodynamics, safety, and preliminary efficacy data. Clin Pharmacol Ther 2000; 68: 556–67.
27 He XL, Yin HL, Wu J, Zhang K, Liu Y, Yuan T, *et al*. A multiple-dose pharmacokinetics of polyethylene glycol recombinant human interleukin-6 (PEG-rhIL-6) in rats. J Zhejiang Univ Sci B 2011; 12: 32–9.
28 Tanaka H, Satake-Ishikawa R, Ishikawa M, Matsuki S, Asano K. Pharmacokinetics of recombinant human granulocyte colony-stimulating factor conjugated to polyethylene glycol in rats. Cancer Res 1991; 51: 3710–4.
29 Bai H, Jing D, Jiang H, Yin S. Pharmacokinetics, tissue distribution and excretion of recombinant human parathyroid hormone 1–84 in animals. Cell Biochem Biophys 2013; 66: 379–87.
30 Song HF, Liu XW, Zhang HN, Zhu BZ, Yuan SJ, Liu SY, *et al*. Pharmacokinetics of His-tag recombinant human endostatin in Rhesus monkeys. Acta Pharmacol Sin 2005; 26: 124–8.
31 Yang XX, Hu ZP, Chan E, Duan W, Zhou S. Pharmacokinetics of recombinant human endostatin in rats. Curr Drug Metab 2006; 7: 565–76.
32 Molema G, van Veen-Hof I, van Loenen-Weemaes AM, Proost JH, de Leij LF, Meijer DK. Pharmacokinetics and whole body distribution of elastase derived angiostatin (K1-3) in rats. Int J Cancer 2001; 91: 1–7.
33 Xie Y, Zhong G, He H, Fan G, Wu Y. Pharmacokinetics, tissue distribution and excretion of porcine fibrinogen after intraperitoneal injection of a porcine-derived fibrin glue to rats. J Pharm Biomed Anal 2011; 54: 148–53.